Biomedical Optics EXPRESS

Minimizing projection artifacts for accurate presentation of choroidal neovascularization in OCT micro-angiography

Anqi Zhang, Qinqin Zhang, and Ruikang K. Wang*

University of Washington, Department of Bioengineering, Seattle, Washington 98195, USA

**wangrk@uw.edu*

Abstract: Current optical coherence tomography (OCT) based micro-angiography is prone to a projection (or tailing) effect due to the high scattering property of blood within overlying patent vessels, creating artifacts that interfere with the interpretation of retinal angiographic results. In this work, the projection effect in OCT micro-angiography is examined and its causality is explained by strong light scattering and photon propagation within blood. A simple practical approach is then introduced to minimize these artifacts presented in the outer retinal avascular space, especially useful for examining clinical cases with choroidal neovascularization (CNV). Demonstrated through *in-vivo* human posterior eye imaging of healthy and CNV subjects, the proposed method is shown effective to eliminate the projection artifacts in outer retinal space of OCT micro-angiography, resulting in better visualization of the pathological neovascularization when compared with the current common approaches. In addition, it is also shown that the proposed method is applicable to minimize the projection artifacts appearing in deep retinal layers.

OCIS codes: (170.4500) Optical coherence tomography; (170.4470) Ophthalmology; (170.3880) Medical and biological imaging.

References and links

1. J. Ambati, B. K. Ambati, S. H. Yoo, S. Ianchulev, and A. P. Adamis, "Age-Related Macular Degeneration: Etiology, Pathogenesis, and Therapeutic Strategies," Surv. Ophthalmol. **48**(3), 257–293 (2003).
2. T. Y. Wong, K. Ohno-Matsui, N. Leveziel, F. G. Holz, T. Y. Lai, H. G. Yu, P. Lanzetta, Y. Chen, and A. Tufail, "Myopic choroidal neovascularisation: current concepts and update on clinical management," Br. J. Ophthalmol. **99**(3), 289–296 (2015).
3. I. Fukushima, K. Kusaka, K. Takahashi, N. Kishimoto, T. Nishimura, H. Ohkuma, and M. Uyama, "Comparison of indocyanine green and fluorescein angiography of choroidal neovascularization," Jpn. J. Ophthalmol. **41**(5), 284–296 (1997).
4. P. E. Stanga, J. I. Lim, and P. Hamilton, "Indocyanine green angiography in chorioretinal diseases: indications and interpretation: an evidence-based update," Ophthalmology **110**(1), 15–23 (2003).
5. M. P. López-Sáez, E. Ordoqui, P. Tornero, A. Baeza, T. Sainza, J. M. Zubeldia, M. L. Baeza, and M. L. Baeza, "Fluorescein-Induced Allergic Reaction," Ann. Allergy Asthma Immunol. **81**(5), 428–430 (1998).
6. Y. Li, U. Baran, and R. K. Wang, "Application of Thinned-Skull Cranial Window to Mouse Cerebral Blood Flow Imaging Using Optical Microangiography," PLoS One **9**(11), e113658 (2014).
7. U. Baran, Y. Li, and R. K. Wang, "Vasodynamics of pial and penetrating arterioles in relation to arteriolo-arteriolar anastomosis after focal stroke," Neurophotonics **2**(2), 025006 (2015).
8. S. Dziennis, J. Qin, L. Shi, and R. K. Wang, "Macro-to-micro cortical vascular imaging underlies regional differences in ischemic brain," Sci. Rep. **5**, 10051 (2015), doi:10.1038/srep10051.
9. M. R. Thorell, Q. Zhang, Y. Huang, L. An, M. K. Durbin, M. Laron, U. Sharma, P. F. Stetson, G. Gregori, R. K. Wang, and P. J. Rosenfeld, "Swept-Source OCT Angiography of Macular Telangiectasia Type 2," Ophthalmic Surg. Lasers Imaging Retina **45**(5), 369–380 (2014).
10. D. Y. Kim, J. Fingler, R. J. Zawadzki, S. S. Park, L. S. Morse, D. M. Schwartz, S. E. Fraser, and J. S. Werner, "Optical imaging of the chorioretinal vasculature in the living human eye," Proc. Natl. Acad. Sci. U.S.A. **110**(35), 14354–14359 (2013).

#246804 Received 27 Jul 2015; revised 16 Sep 2015; accepted 17 Sep 2015; published 28 Sep 2015

11. J. Qin, J. Jiang, L. An, D. Gareau, and R. K. Wang, "In vivo volumetric imaging of microcirculation within human skin under psoriatic conditions using optical microangiography," Lasers Surg. Med. **43**(2), 122–129 (2011).
12. W. J. Choi, H. Q. Wang, and R. K. Wang, "OCT microangiography for monitoring the response of vascular perfusion to external pressure on human skin tissue," J. Biomed. Opt. **19**(5), 056003 (2014).
13. B. J. Vakoc, D. Fukumura, R. K. Jain, and B. E. Bouma, "Cancer imaging by optical coherence tomography: preclinical progress and clinical potential," Nat. Rev. Cancer **12**(5), 363–368 (2012).
14. Y. J. Hong, M. Miura, S. Makita, M. J. Ju, B. H. Lee, T. Iwasaki, and Y. Yasuno, "Noninvasive investigation of deep vascular pathologies of exudative macular diseases by high-penetration optical coherence angiography," Invest. Ophthalmol. Vis. Sci. **54**(5), 3621–3631 (2013).
15. D. M. Schwartz, J. Fingler, D. Y. Kim, R. J. Zawadzki, L. S. Morse, S. S. Park, S. E. Fraser, and J. S. Werner, "Phase-variance optical coherence tomography: a technique for noninvasive angiography," Ophthalmology **121**(1), 180–187 (2014).
16. E. Moult, W. Choi, N. K. Waheed, M. Adhi, B. Lee, C. D. Lu, V. Jayaraman, B. Potsaid, P. J. Rosenfeld, J. S. Duker, and J. G. Fujimoto, "Ultrahigh-Speed Swept-Source OCT Angiography in Exudative AMD," Ophthalmic Surg. Lasers Imaging Retina **45**(6), 496–505 (2014).
17. T. Lindmo, D. J. Smithies, Z. Chen, J. S. Nelson, and T. E. Milner, "Accuracy and noise in optical Doppler tomography studied by Monte Carlo simulation," Phys. Med. Biol. **43**(10), 3045–3064 (1998).
18. S. Makita, Y. Hong, M. Yamanari, T. Yatagai, and Y. Yasuno, "Optical coherence angiography," Opt. Express **14**(17), 7821–7840 (2006).
19. B. J. Vakoc, R. M. Lanning, J. A. Tyrrell, T. P. Padera, L. A. Bartlett, T. Stylianopoulos, L. L. Munn, G. J. Tearney, D. Fukumura, R. K. Jain, and B. E. Bouma, "Three-dimensional microscopy of the tumor microenvironment in vivo using optical frequency domain imaging," Nat. Med. **15**(10), 1219–1223 (2009).
20. A. Zhang and R. K. Wang, "Feature space optical coherence tomography based micro-angiography," Biomed. Opt. Express **6**(5), 1919–1928 (2015).
21. R. K. Wang, "Signal degradation by multiple scattering in optical coherence tomography of dense tissue: A Monte Carlo study towards optical clearing of biotissues," Phys. Med. Biol. **47**(13), 2281–2299 (2002).
22. E. Jonathan, J. Enfield, and M. J. Leahy, "Correlation mapping method for generating microcirculation morphology from optical coherence tomography (OCT) intensity images," J. Biophotonics **4**(9), 583–587 (2011).
23. J. Fingler, D. Schwartz, C. Yang, and S. E. Fraser, "Mobility and transverse flow visualization using phase variance contrast with spectral domain optical coherence tomography," Opt. Express **15**(20), 12636–12653 (2007).
24. L. An, J. Qin, and R. K. Wang, "Ultrahigh sensitive optical microangiography for in vivo imaging of microcirculations within human skin tissue beds," Opt. Express **18**(8), 8220–8228 (2010).
25. R. K. Wang, L. An, P. Francis, and D. J. Wilson, "Depth-resolved imaging of capillary networks in retina and choroid using ultrahigh sensitive optical microangiography," Opt. Lett. **35**(9), 1467–1469 (2010).
26. Y. Jia, O. Tan, J. Tokayer, B. Potsaid, Y. Wang, J. J. Liu, M. F. Kraus, H. Subhash, J. G. Fujimoto, J. Hornegger, and D. Huang, "Split-spectrum amplitude-decorrelation angiography with optical coherence tomography," Opt. Express **20**(4), 4710–4725 (2012).
27. A. Mariampillai, B. A. Standish, E. H. Moriyama, M. Khurana, N. R. Munce, M. K. K. Leung, J. Jiang, A. Cable, B. C. Wilson, I. A. Vitkin, and V. X. D. Yang, "Speckle variance detection of microvasculature using swept-source optical coherence tomography," Opt. Lett. **33**(13), 1530–1532 (2008).
28. V. V. Tuchin, X. Xu, and R. K. Wang, "Dynamic optical coherence tomography in studies of optical clearing, sedimentation, and aggregation of immersed blood," Appl. Opt. **41**(1), 258–271 (2002).
29. M. Friebel, A. Roggan, G. Müller, and M. Meinke, "Determination of optical properties of human blood in the spectral range 250 to 1100 nm using monte carlo simulations with hematocrit-dependent effective scattering phase functions," J. Biomed. Opt. **11**(3), 034021 (2006).
30. G. Liew, J. J. Wang, P. Mitchell, and T. Y. Wong, "Retinal vascular imaging: a new tool in microvascular disease research," Circ Cardiovasc Imaging **1**(2), 156–161 (2008).
31. X. Yin, J. R. Chao, and R. K. Wang, "User-guided segmentation for volumetric retinal optical coherence tomography images," J. Biomed. Opt. **19**(8), 086020 (2014).
32. M. S. Mahmud, D. W. Cadotte, B. Vuong, C. Sun, T. W. Luk, A. Mariampillai, and V. X. Yang, "Review of speckle and phase variance optical coherence tomography to visualize microvascular networks," J. Biomed. Opt. **18**(5), 050901 (2013).

1. Introduction

Choroidal neovascularization (CNV) involves the growth of abnormal new blood vessels that originate from choroid, breaking through Bruch's membrane (BM) and extending into the retinal pigment epithelium (RPE) and outer retinal space. CNV is a major cause of vision loss and impairment involved in a number of retinal pathologies such as, e.g., age-related macular degeneration (AMD) [1] and high myopia [2]. Early detection and monitoring of CNV is crucial to the control of disease progression. Fluorescein angiography (FA) and indocyanine green angiography (ICGA) have been *de facto* the golden standard for detecting

#246804 Received 27 Jul 2015; revised 16 Sep 2015; accepted 17 Sep 2015; published 28 Sep 2015

neovascularization within retina and choroid in ophthalmic clinic. Both FA and ICGA have proven their clinical usefulness for patients with CNV [3]. However, none of these methods is depth resolved; hence they have to rely on clinician's judgement to differentiate the neovascularization characterized by CNV. Furthermore, both FA and ICGA require intravenous dye injection, which might result in nausea and other side effects [4, 5], and more importantly cannot be used repeatedly on patients over time.

Optical coherence tomography (OCT) micro-angiography (OCTA) is a new imaging modality providing visualization of three dimensional (3D) blood vessel networks, without a need for exogenous contrast agents. In part due to this attribute, OCT micro-angiography promises to be a valuable imaging tool in the examination of pathological neovascularization with respect to its localized depth information. OCTA has now been widely used in the imaging of cerebrovascular perfusion [6–8], retinal microcirculation [9,10], skin conditions [11,12] and tumor progression [13] etc. In ophthalmic imaging, OCTA has already been demonstrated useful to visualize and monitor CNVs [14–16], potentially providing additional critical information in clinical decision making. However it is noticed that in OCTA there is undesired projection effect from overlying blood vessels that leads to strong image artifacts appearing in the results of blood vessel networks within outer retinal space and choroid. These artifacts limit our ability to visualize and interpret 3D angiographic results. Though it was not until recent years that the projection artifacts in OCTA became well noticed by clinicians and physicians, Lindmo *et al.* in 1998 discussed the stochastic Doppler frequency noise as shadowing artifacts in the framework of time domain Doppler OCT [17]. Later Makita *et al.* mentioned a method utilizing retinal vessels to reduce the shadowing artifacts presented in choroidal vessel visualization when applying phase-resolved Doppler OCT [18]. Recently Vakoc *et al.* proposed a step-down exponential filtering to attenuate all the signals below overlying vessels during vessel tracing in post-processing [19].

Furthermore in the diagnosis of CNV cases, it is often required to examine whether new blood vessels arising from choroid are breaking through the BM or RPE, upon which to differentiate the type I from the type II CNVs. On the other hand in the therapeutic intervention of CNV, it is imperative to have an ability for clinicians to assess in detail how the CNV within outer retinal space responds to therapy. Anatomically, the outer retinal space discussed in this paper is defined as the space encompassing regions from outer nuclear layer (ONL) to BM, where there should not appear any functional blood vessels for normal subjects. This space is often called avascular space in the human retina. However, the OCT micro-angiography of the outer retinal space often shows strong signals even in the case of normal human subjects where it should be avascular. These projection artifacts resemble the overlying retinal blood vessels and are prominent at the inner and outer photoreceptor segments (IS/OS) and RPE layers due to their hyper-reflective nature in OCT signals. Clearly, these projection artifacts greatly impede our ability to interpret OCTA results in the above mentioned clinical CNV scenarios. Currently, approach in dealing with this issue of projection artifacts is simply to exclude the signals from IS/OS and RPE layers from the final results, often through segmentation. Such treatment, although sometimes effective in the terms of visualization, is questionable as to whether the outcome identifies complete pathological neovasculature within outer retinal avascular space.

The purpose of this present work is to introduce practical solutions to minimize the artifacts from projection effects due to the overlying retinal blood vessels without excluding the IS/OS and RPE layers from the OCTA of outer retinal space. In the rest of this paper, section 2 discusses the possible causes of projection effect phenomenon in some detail. Section 3 describes a simple method to eliminate/minimize the projection artifacts in *in-vivo* human CNV cases. Throughout this work, we use our newly developed feature space optical micro-angiography (fsOMAG) to deliver the angiographic results in favor of its resistance to static background signals [20]. However, as discussed below, such method of mitigating the

#246804 Received 27 Jul 2015; revised 16 Sep 2015; accepted 17 Sep 2015; published 28 Sep 2015

projection artifacts is not exclusive to fsOMAG but universal to the current family of OCT based angiography.

2. The projection effect in OCT based angiography

To begin with, all the clinical data used in this work were obtained from a clinical investigational study where a 67 kHz Cirrus angiography prototype spectral-domain OCT system (central wavelength = 840 nm, and full width at half maximum = 45 nm) (Carl Zeiss Meditec Inc, Dublin, CA) was used to image the enrolled patients. In the study, each volumetric data set covered a 2.4 mm by 2.4 mm scanning area centered at the fovea. 980 B-scans were acquired from 245 transversal locations with 4 repetitions at each location. Each single B-scan consists of 245 A-scans. For each A-scan, 1024 sampling points were generated along a 2.0 mm axial scan depth. The time difference between two successive B-scans was roughly 3.7 ms, which corresponds to a B-scan acquisition rate of 270 B-scans per second. The Institutional Review Board of University of Washington reviewed and approved the clinical investigational study, and informed consent was obtained from all subjects before imaging. This study followed the tenets of the Declaration of Helsinki and was conducted in compliance with the Health Insurance Portability and Accountability Act.

The projection artifact is widespread in OCT based angiography and results in an appearance of "false" blood flow signals in the tissue regions that in fact should be avascular. This projection artifact is sometimes referred to as the "tailing artifact". One typical example is illustrated in Fig. 1, where Fig. 1(a) is a representative structural OCT image by taking average of the four repeated scans, and Fig. 1(b) is the corresponding angiographic image (i.e., blood flow image). The tailing effect behind functional blood vessels can be firstly observed in the figures as the elliptic-like shape of blood vessels as indicated by the yellow cycles. This appearance may be explained by light scattering and photon propagation within the blood tissue [21]. In OCT, it is known that the light scattering, more precisely the light backscattering at depths, gives the contrast of OCT signal. When light propagates within a functional blood vessel, the blood strongly scatters the incoming photons of probe beam due to the highly scattering nature of the blood [i.e., red blood cells (RBC)]. Part of the photons is likely to have been scattered multiple times before they are backscattered and detected by the OCT system through its coherence gate. Compared with ballistic photons backscattered at the same location, those photons experiencing multiple scattering events would have increased optical pathlength. Since OCT displays the depth resolved information according to the optical pathlength difference between the sample and reference arms, it is then not difficult to appreciate that these multiply scattered photons are responsible for the elongated shape of blood vessels that appear in both the cross-sectional structural image and corresponding angiographic image. However, this type of projection effect may only locally affect the shape of blood vessels and is not expected to impact on the angiographic results anywhere else.

The second type of projection effect leads to "false" flow signal at places where it should otherwise have no flow signal at all. As indicated by the red arrows in Fig. 1(b), false signals are observed at the IS/OS and RPE tissue complex by considering the fact that this tissue complex is avascular (in normal subjects). It is noted that there were many other locations along the RPE layer where projection artifacts were obvious. Only two locations were selected for clarity in the figure. The same locations on the structural image were also marked by the red arrows as in Fig. 1(a). This type of projection effect would contaminate the angiographic results of outer retinal space and cause problems especially when the results are presented in an enface view according to the locations along depth. We now refer the projection effect only to this 2nd type throughout the text that follows, which is to be tackled with as the focus of this study in order to improve our ability in the interpretation of CNV images provided by OCT micro-angiography.

#246804 Received 27 Jul 2015; revised 16 Sep 2015; accepted 17 Sep 2015; published 28 Sep 2015

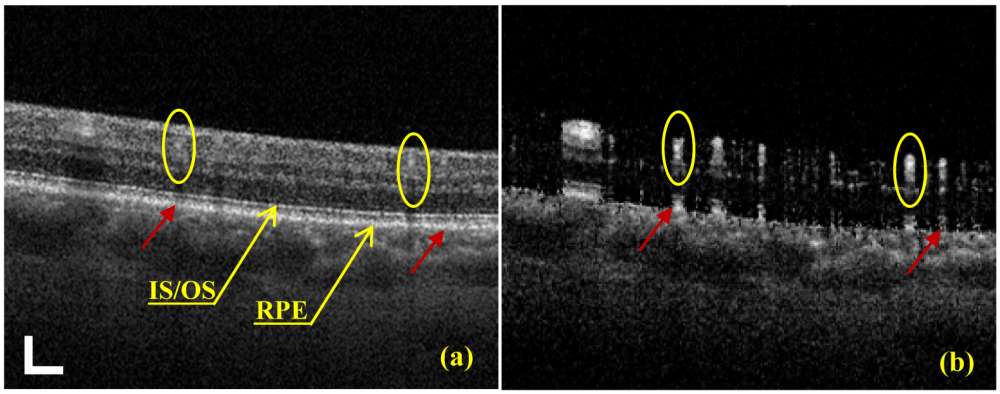

Fig. 1. Example of projection effect. (a) Cross-sectional OCT B-scan image; and (b) corresponding angiographic results by the use of fsOMAG. The yellow circles denote elongated blood vessel shape indicating the first type of projection effect. The red arrows denote the artifacts in the RPE complex, which would make it difficult to interpret the angiography of outer retinal space. Scale bar: 200 μm.

Firstly, a careful comparison among the OCT signals of projection artifacts in the RPE layer in Fig. 1(a) indicates that projection effect leads to decreased intensity (i.e., shadows) in the structural image. This is due to the strong absorption of the blood within patent vessels located within the retinal layers. However, the signal strengths at the locations, where red arrows point in Fig. 1(a), also tell that the projection effect does not necessarily lead to a decrease in intensity. Secondly, it is observed that at the junctions of IS/OS and RPE in Fig. 1(a), there is not a noticeable change in curvature at where projection effect occurs. This indicates that this type of artifacts is very likely not caused by the change in optical path length due to multiple scattering events (as described in the 1st type of projection effect above). Thus, we can conclude that the multiple scattering of photons within blood should not play a crucial role in the projection effect of this 2nd type.

To study the creation of the projection effect of this 2nd type, we consider the nature of the complex OCT signal in Fourier domain OCT, including spectral domain and swept source configurations. The complex signal has two components, i.e. its magnitude and its phase. From the scanning protocol of OCT micro-angiography, we analyze the changes in both magnitudes (speckle pattern) and phases among four repeated B-scans. In doing so, hereby we choose intensity decorrelation [22] due to its normalization operation, which reduces the influence of intensity values when evaluating the difference, and phase variance [23] to denote the changes in magnitude and phase among repeated B-scan measurements. The same transversal location as shown in Fig. 1 was examined. The results are illustrated in Figs. 2(a) and 2(b) after applying the algorithms of decorrelation and phase variance, respectively. The corresponding locations that are marked by red arrows in Fig. 1 are also indicated in Figs. 2(a) and 2(b). It can be seen that at the locations where projection effect occurs, both the magnitude and the phase signals have high variance among repeated measurements. Consequently, it would be also true for the complex OCT signals at these locations (Fig. 1(b)). This fact implies that it would be difficult for all the current OCTA algorithms to directly differentiate the projection artifacts from the true blood vessel signals. These algorithms include, but are not limited to, complex OCT signal based approach, such as OMAG [24, 25]; magnitude based approach, such as decorrelation [22], SSADA [26] and speckle variance [27]; and phase based approach, e.g. phase variance [23].

#246804 Received 27 Jul 2015; revised 16 Sep 2015; accepted 17 Sep 2015; published 28 Sep 2015

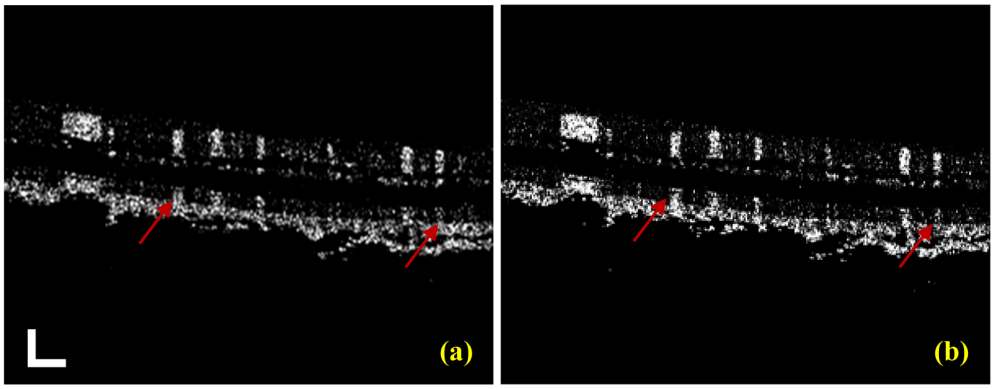

Fig. 2. The projection effect appeared in both magnitude and phase based variance algorithms. (a) The intensity decorrelation results of the same transversal position as in Fig. 1, and (b) corresponding phase variance results. The red arrows indicate both high decorrelation value and phase variance at the locations where the projection effect occurs. Scale bar: 200 μm.

From the above, two statements can be made regarding the photons backscattered at the locations where projection effect occurs: 1) The detected photons do not experience significant changes in their optical pathlength after being multiply scattered within blood (relative to the optical pathlength of the ballistic photons); and 2) they induce large variance in the magnitude and phase of OCT signals. Such conclusions lead to a speculation that when photons pass through a functional blood vessel, they undergo forward-scattering events after interacting with moving RBCs. This is not a surprise because erythrocytes in blood vessels are of very high anisotropy factor ($g>0.99$ at the OCT wavelength range), hence would strongly forward-scatter the incoming photons [28, 29]. Those photons that are strongly forward-scattered by the RBCs may not induce a noticeable change in their optical pathlength after escaping from the blood vessel and captured by OCT system because: 1) the angular deviation of the scattering direction with respect to the incoming photon direction is very small due to $g>0.99$, and 2) the coherence gating of the OCT system makes sure that the received photons at one depth are only backscattered within a very tight cone towards the detector (which may be explained by the product of the numerical aperture of detection with the coherence gate). However, these captured photons have already been scattered by the moving RBCs, which would lead to at least two consequences: 1) a change in the phase of OCT signal due to Doppler effect, and 2) a change in the OCT signal magnitude due to a change in reflectivity / refractivity of moving RBC relative to the probe beam. Since the final depth-resolved OCT signal is determined by the coherent contribution of all the backscattered photons along the depth, the outcome would eventually lead to a large variation in intensity and phase of the OCT signals. As a result, the localization of these forward-scattered photons enabled by the coherence gating leaves a trail behind the functional blood vessel. This phenomenon is more obvious when there are high-reflecting interfaces beneath the vessel, e.g. IS/OS and RPE.

Figure 3 explains the random OCT signal considered at one certain depth d. The induced Doppler phase shifts from the forward scattering events lead to θ as the angle of $\vec{v}_{bs}$ representing the backscattering event captured by coherence gating at depth d. The magnitude of $\vec{v}_{bs}$ is determined by the product of moving RBC refractivity and backscattering coefficient at the depth d. The contribution of the static tissue at the depth d is denoted as $\vec{v}_{other}$. The obtained OCT signal is therefore $\vec{v}_{OCT}$ as illustrated in Fig. 3. Hence, the change in θ and in magnitude of the OCT signal within each repeated measurement lead to intensity and phase variations among repeated scans at places where the projection effect occurs.

#246804 Received 27 Jul 2015; revised 16 Sep 2015; accepted 17 Sep 2015; published 28 Sep 2015

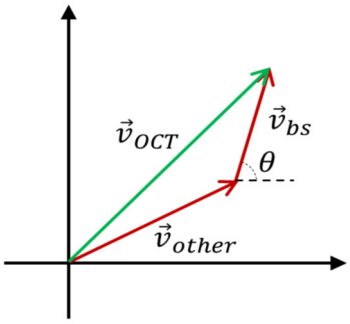

Fig. 3. The illustration of OCT signal at one depth determined coherently by the contributions of all the backscattered photons.

3. Practical approach to minimize projection artifacts in visualizing CNV

For typical CNV cases, the newly developed vessels break through BM into outer retinal space. The projection effect described in the Section 2 gives obvious artifacts beneath retinal tissue in the IS/OS and RPE tissue complex, which can overlap with the true signals from new abnormal blood vessels. Such artifacts have given difficulties to interpret the angiographic results of outer retinal avascular space (ORAS). Below we introduce practical solutions to mitigate the interference of the projection artifacts in the interpretation of OCT micro-angiography of ORAS. First of all, we describe some definitions to facilitate the discussion. The ORAS is defined as the space between the outer plexiform layer (OPL) to the BM, where it should be avascular, and the retinal space is defined as the region from the inner limiting membrane (ILM) to the OPL including OPL. Superficial retinal layer is defined as the region from the ILM to the inner plexiform layer (IPL) including IPL, and a deep retinal layer from the inner nuclear layer (INL) to the OPL including OPL.

As discussed above, the projection artifacts appearing in the ORAS are due to the functional blood vessels innervating retinal tissue. Therefore, it would be reasonable to utilize the blood vessel information obtained from within retinal space to compensate the blood vessel images acquired from the ORAS. We know that in the current OCT based angiography, the blood vessel images are typically presented by enface visualization through either maximum projection or average projection along depth. And the final images are provided by logarithmic compression in order to reduce the dynamic range of the displayed values for the purpose of enhancing image contrast for weak signals. Suppose the projection image obtained from retina is $A_R(x,y)$, and that from the ORAS is $A_T(x,y)$ *i.e.,* the true signal of interest. Thus, the detected projection image from the ORAS, $A_S(x,y)$, can be approximately written as:

$$A_S(x,y) = A_T(x,y) \cdot \alpha A_R(x,y) \tag{1}$$

where α is a scaling factor that is used to properly scale $A_R(x,y)$ to match the values of $A_T(x,y)$. A logarithmic operation of Eq. (1) gives:

$$\log\left[A_S(x,y)\right] = \log\left[A_T(x,y)\right] + \log\left[\alpha A_R(x,y)\right] \tag{2}$$

Therefore,

$$\log\left[A_T(x,y)\right] = \log\left[A_S(x,y)\right] - \log\left[\alpha A_R(x,y)\right] \tag{3}$$

#246804 Received 27 Jul 2015; revised 16 Sep 2015; accepted 17 Sep 2015; published 28 Sep 2015

Consequently, the true angiographic image for the ORAS can be obtained by a simple subtraction of a scaled image obtained from the retinal space from the image obtained from the ORAS. However, this operation relies on the proper selection of the scaling factor α, which is sometimes case-dependent, thus not desirable for practical operations in clinical systems. To solve this issue, a more practical approach would be to normalize the retinal image into a range of [0 1], and then:

$$\log\left[A_T(x,y)\right] = \log\left[A_S(x,y)\right] \cdot \left\{1 - \mathrm{Norm}\left\langle \log\left[A_R(x,y)\right]\right\rangle\right\} \quad (4)$$

where $\mathrm{Norm}\langle ... \rangle$ denotes normalization operation. This simple treatment does not involve the selection of the scaling factor α and the normalization operation is straightforward, thus, can be easily implemented in the current clinical systems, which is particularly attractive.

On the other hand for most pathological retinal cases, the structural pathological change may precede the development of neovascular growth [30]. Hence, it would be reasonable to consider the retinal structural information into the formulation to further improve the accuracy of projection artifact removal. Here, because our focus is to visualize the CNVs, the structural projection image from the ORAS, $I_S(x,y)$, is used to weigh Eq. (4). Thus, Eq. (4) is re-written as:

$$\log\left[A_T(x,y)\right] = \log\left[A_S(x,y)\right] \cdot \left\{1 - \mathrm{Norm}\left\langle \log\left[A_R(x,y)\right]\right\rangle \cdot \left\{1 - \mathrm{Norm}\left\langle \log\left[I_S(x,y)\right]\right\rangle\right\}\right\} \quad (5)$$

The retinal structural information is readily available in the current clinical OCT systems. Therefore its inclusion would not complicate the evaluation process.

4. Results

Below we demonstrate the proposed practical approach to eliminate the projection artifacts appearing in the outer retinal avascular space. The cases presented include the data sets captured from normal subject and patients diagnosed with CNV and polypoidal choroidal vasculopathy (PCV). As a demonstration, we used the fsOMAG algorithm to process all the data sets to obtain OCT angiographic images. To provide the vascular networks lying within retinal, outer retinal and choroidal spaces, we used a semi-automatic segmentation software developed in house [31], based on intensity difference among different retinal layers in the OCT structural image, to segment the layers of interests.

Figure 4 demonstrates one example of the projection artifact removal by use of the proposed approach (Eq. (5) to process the data set acquired from a healthy subject. Figure 4(a) illustrates one representative B-scan image. The segmentation software was used to delineate the interfaces of ILM, OPL, IS/OS, RPE and BM layers. In Fig. 4(a) we indicate the retinal and outer retinal avascular spaces according to the definitions described in the last section. Accordingly, the subsequent OCTA results are presented in Fig. 4(b) and Fig. 4(c) for retina and outer retinal space, respectively. It is clear that the artifacts due to retinal blood vessels are prominent in the outer retinal space (Fig. 4(c)), where for normal subjects there should have no functional blood vessels. In the current normal practice to get away from this artifact, it is simply to parallel-shift the segmentation line of RPE up to above the IS/OS line (as shown in Fig. 4(a)), and then produce the projection results from OPL to this shifted line to exclude the projection artifacts appeared in the IS/OS and RPE layers. This approach appears the most common way employed for examining the CNV cases. By this approach, the angiographic result is presented in Fig. 4(d), where indeed the appearance of OCTA image is avascular. However such avascular appearance does not necessarily represent the avascular space in the retina as demonstrated in the CNV cases below.

#246804 Received 27 Jul 2015; revised 16 Sep 2015; accepted 17 Sep 2015; published 28 Sep 2015

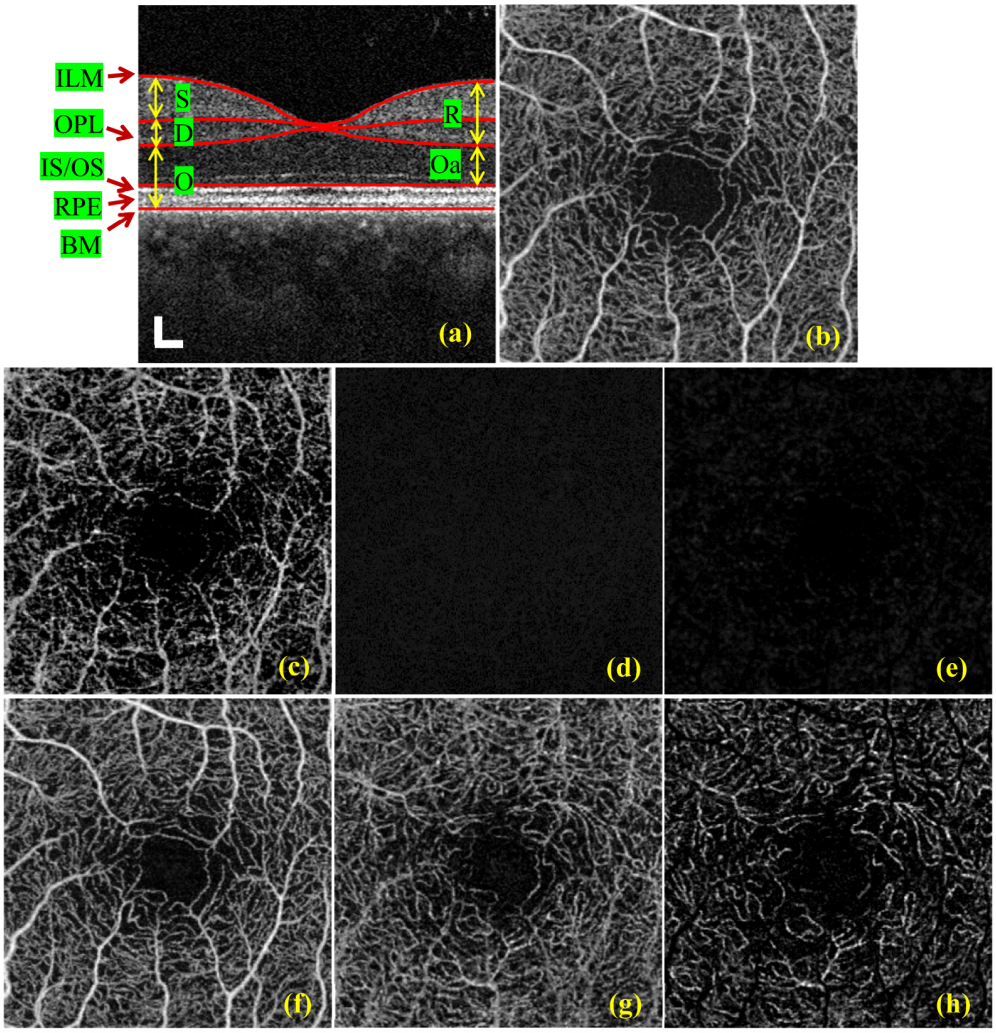

Fig. 4. Demonstration of the removal of projection artifacts using the data set acquired from a healthy subject. (a) Representative B-scan image indicating the inner retina and outer retina; S: Superficial retina; D: Deep retina; R: Retinal space; O: Outer retinal space; Oa: Outer retina above IS/OS. Scale bar: 200 μm; (b) Retinal vasculature network, that is used removal of projection artifacts; (c) Direct result obtained from outer retinal avascular space; (d) Result obtained by excluding the signals from IS/OS and RPE; (e) Results from outer retinal avascular space after removal of projection artifacts; (f) Superficial retinal vascular network; (g) Direct results of the deep retinal layer; and (h) Results of the deep retinal layer after removal of projection artifacts.

To obtain true representation of OCTA of avascular space, we applied the proposed approach as described in the last section, where the retinal vascular image of Fig. 4(b) was used to compensate the obtained avascular image of Fig. 4(c). The result is presented in Fig. 4(e), where it can be seen that most of the artifacts in the outer retina are removed, demonstrating the effectiveness of the proposed approach to eliminate/minimize the projection artifacts.

Further, it is interesting to examine the vasculature of the deep retinal layer obtained by OCTA, which also suffers from the projection artifacts from the superficial retinal layer. Figures 4(g) and 4(h) illustrate OCTA results of the deep retinal vasculature before and after projection artifacts removal, respectively. In this case, the angiographic result of the

#246804 Received 27 Jul 2015; revised 16 Sep 2015; accepted 17 Sep 2015; published 28 Sep 2015

superficial retinal vessels [Fig. 4(f)] was normalized to compensate the projection artifacts in the image of the deep retinal layer using Eq. (4). Compared with Fig. 4(g), Fig. 4(h) is seen without projection artifacts from Fig. 4(f), demonstrating that the proposed method would be also applicable to the deep retinal layers.

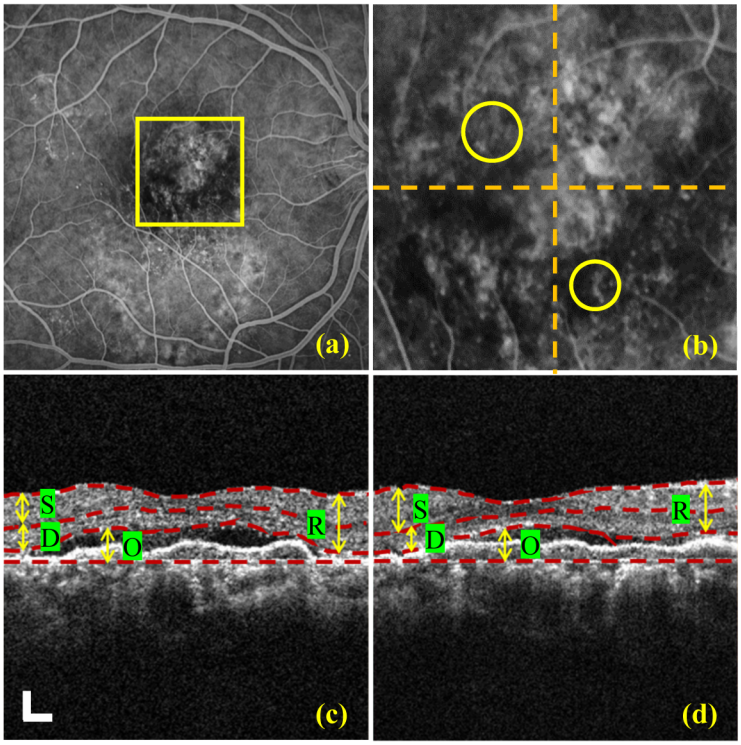

Fig. 5. The FA and OCT images of Type 1 CNV case. (a) The FA image of a 50-year-old woman (right eye). The yellow box denotes the OCT micro-angiography scanning area; (b) The zoomed OCT scanning area; (c) OCT B-scan image corresponding to the location indicated by the horizontal yellow dashed line in (b); (d) OCT B-scan image corresponding to the location indicated by the vertical yellow dashed line in (b); S: Superficial retina; D: Deep retina; R: Retinal space; O: Outer retina. Scale bar: 200 μm.

Figures 5 and 6 demonstrate one CNV case employing projection artifact removal in a 50-year-old woman diagnosed with Type 1 CNV in age-related macular degeneration (right eye). Figure 5(a) shows the FA image, where the yellow box indicates the scanned area for OCT micro-angiography. This OCT scanning area is zoomed and displayed in Fig. 5(b) for better comparison. Figures 5(c) and 5(d) illustrate the OCT B-scan structural images at the locations denoted by the horizontal and vertical yellow dashed lines in Fig. 5(b), respectively. The FA images in Fig. 5(a) and 5(b) indicate outer retinal neovascularization, which is also manifested by the irregular shape of the RPE and the existence of OCT signals between RPE and BM in the OCT B-scans in Figs. 5(c) and 5(d).

Figures 6(a) illustrates the OCT angiographic results of the entire outer retina up to BM, where the CNV is clearly demonstrated. Because the RPE layer has not been penetrated as seen in Figs. 5(c) and 5(d), this CNV can be classified as the Type I. Notwithstanding, the OCTA vascular image of this space is heavily contaminated by the projection artifacts as evidenced in Fig. 6(a), giving problems to accurately interpret and examine the extent of the CNV in this case. Because most projection artifacts are the false signals due to the reflections of IS/OS and RPE, segmentation would help reduce these false signals. In doing so, we produced the results by excluding the signals from IS/OS and RPE layers as shown in Fig.

#246804 Received 27 Jul 2015; revised 16 Sep 2015; accepted 17 Sep 2015; published 28 Sep 2015

6(b), where it can be seen that the projection artifacts are reduced to some extent. The residual artifact is due to segmentation errors because of irregular shape of RPE as seen in Fig. 5. Unfortunately the CNV appearance is almost gone, which would affect the clinical interpretation of the results, meaning that such approach of excluding IS/OS and RPE signals in the final results would not be always effective. Therefore, the accurate examination of CNV requires the OCTA to produce the results of entire avascular space.

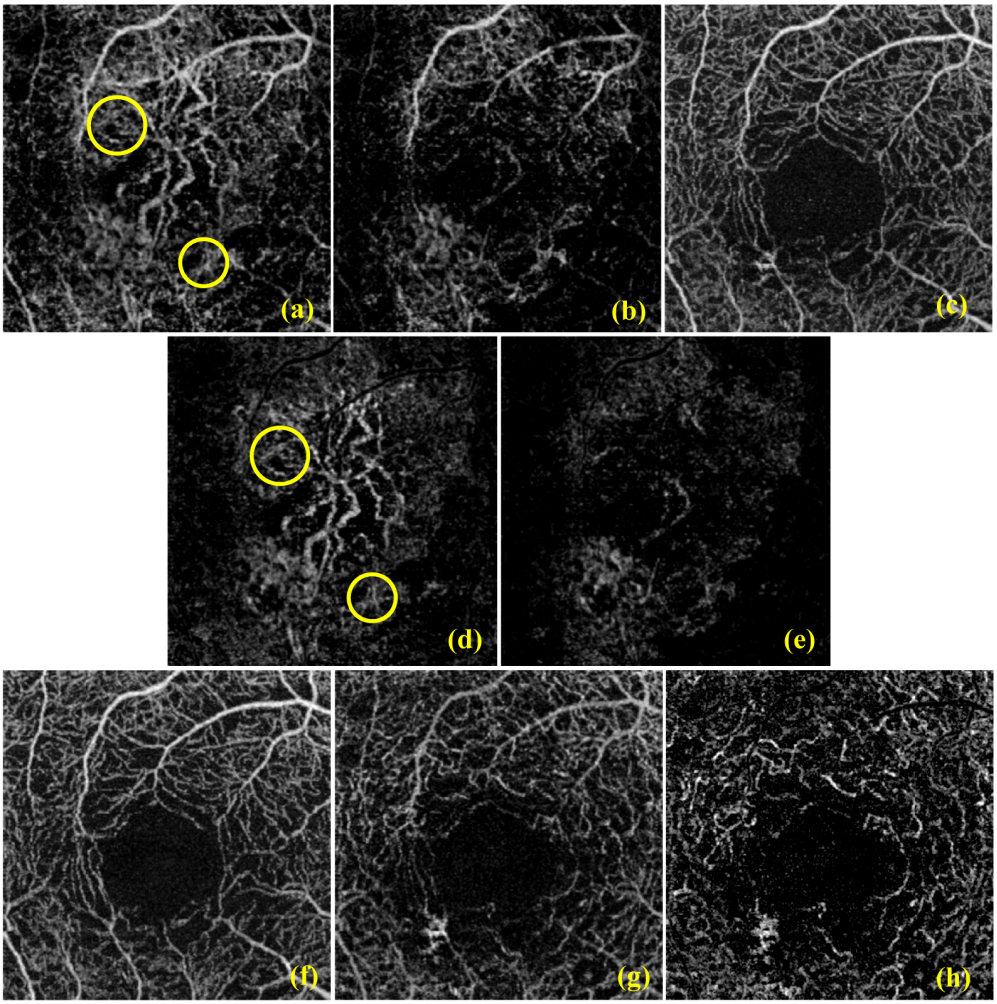

Fig. 6. The OCT micro-angiography of the Type 1 CNV case over the area indicated by the yellow box in Fig. 5(a). (a) Direct OCTA of the entire outer retina; (b) Direct OCTA of the outer retinal space but above the IS/OS; (c) OCTA of retinal space; (d) OCTA of the outer retinal space after removing the projection artifacts due to retinal vessels; (e) OCTA of the outer retina but above the IS/OS after removing the projection artifacts due to retinal vessels; (f) OCTA of the superficial retinal layer; (g) OCTA of the deep retinal layer; (h) OCTA of the deep retinal layer after projection artifact removal.

Figure 6(c) illustrates the OCTA result of retinal space and Fig. 6(d) gives the OCTA results of entire outer retina after applying the proposed approach to remove projection artifacts. Comparing Figs. 6(a) and 6(d), it clearly indicates that the proposed approach effectively removes the artifacts, which might otherwise confound the diagnosis. In particular, the vascular patterns indicated by yellow circles are obvious in Fig. 6(d), which agree well with that of FA image [yellow circles in Fig. 5(b)]. However, it is difficult to identify these

#246804 Received 27 Jul 2015; revised 16 Sep 2015; accepted 17 Sep 2015; published 28 Sep 2015

patterns as pathological neovasculature in Fig. 6(a) due to the contamination of the projection artifacts. This, on the other hand, demonstrates the usefulness of the proposed artifact removal approach.

In addition, the proposed algorithm was applied to the image presented in Fig. 6(b), which was obtained by excluding the false signals due to IS/OS and RPE. The result is shown in Fig. 6(e), where it is also evident that the projection artifacts are effectively removed. However, the resulted OCTA only demonstrates a small portion of CNV in this case, which is not desirable for accurate clinical assessment, indicating the importance to include all the signals within the space from ONL to BM to examine the whole extent of CNV.

Next we also examined the OCTA image of the deep retinal layer before and after projection artifact removal by using the superficial retinal vessels [Fig. 6(f)]. The results are illustrated in Fig. 6(g) and 6(h), respectively. It is indicated in Fig. 6(h) that the deep retinal vasculature can be better visualized by the exclusion of projection artifacts.

Figure 7 illustrates another CNV case by employing the proposed approach to remove projection artifacts. The data sets were acquired from a 50-year-old woman with PCV (left eye). Figures 7(a) and 7(b) show the ICGA images of early and late stages, respectively, demonstrating the growth of new blood vessels within polyps. The yellow box in Fig. 7(b) indicates OCT micro-angiography scanning area. Figure 7(c) shows the FA image and Fig. 7(d) is the wide-field OCT B-scan image at the location indicated by the green line in Fig. 7(c). The branching network of PCV can be identified in the late stage of ICGA image in Fig. 7(b) and FA image in Fig. 7(c) as the hyper-fluorescent region. The wide-field OCT image in Fig. 7(d) also indicates the disease by a dome-like elevation (pointed by yellow arrow) of RPE, which is the polyp within which the growth of new blood vessel occurs. Figures 7(e) and 7(f) illustrate the OCTA results of the outer retina before and after the removal of projection artifacts, respectively. Both images demonstrate directly the abnormal neovasculature within polyp. However, the result after applying the proposed approach shows a much cleaner neovasculature network with no obvious projection artifacts, which we believe would be useful in the clinical diagnosis and treatment monitoring of this type of disease.

5. Discussion and conclusions

Projection artifacts are obvious in OCT based angiography, which can interfere with the clinical interpretation of the final angiographic results. The proposed artifacts removal algorithm considers both the overlying layer vasculature and OCT structural information, which is based on two facts: 1) The projection artifacts resemble the vasculature of the overlying layers; and 2) The growth of pathological new vasculature is concurrent with the change in tissue structure. In the case when neovasculature is contaminated with projection artifacts, simple subtraction approach, i.e., Eq. (3) or Eq. (4), would affect the appearance of neovasculature. Such problem is solved, at least in part, by considering the structural information. The proposed method works well for the presented cases in this work.

#246804 Received 27 Jul 2015; revised 16 Sep 2015; accepted 17 Sep 2015; published 28 Sep 2015

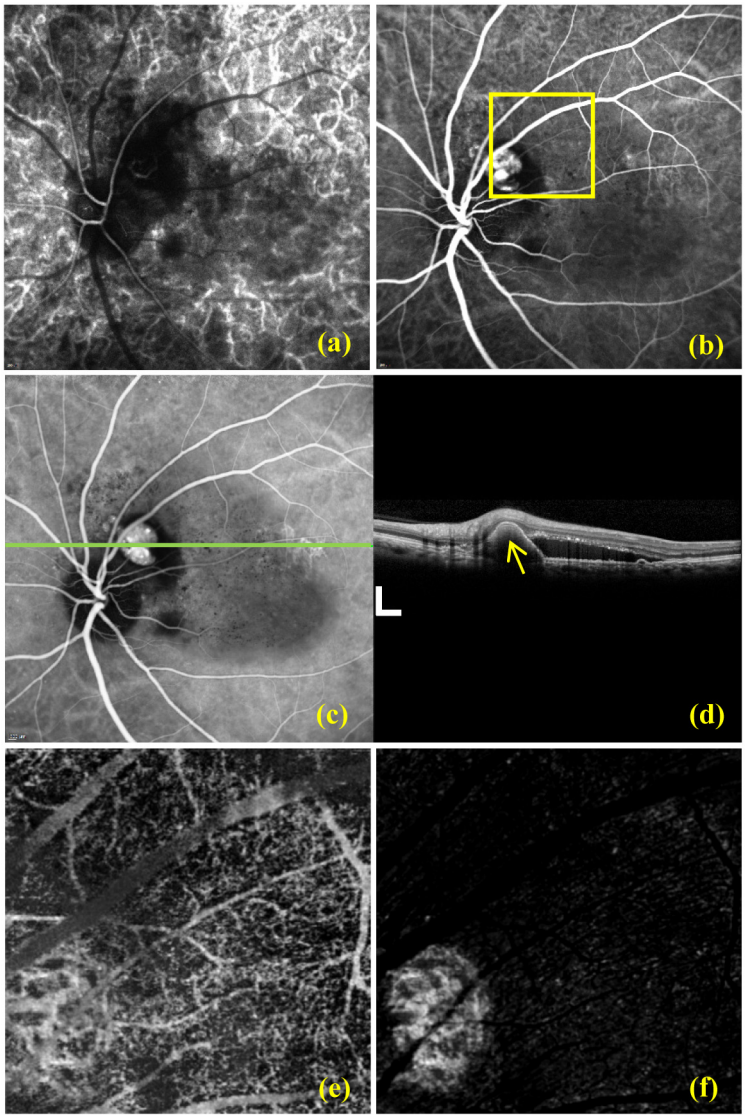

Fig. 7. The OCTA of CNV case of a 50-year-old woman diagnosed with PCV (left eye). (a) The early stage ICGA; (b) The late stage ICGA with the yellow box denoting the OCT micro-angiography scanning area; (c) The FA image; (d) The wide-field OCT B-scan image at the location indicated by the green line in Fig. 7(c); Scale bar: 500 μm; (e) OCT angiographic results before and (f) after applying the algorithm to remove projection artifacts.

It is noticed that the issues of shadowing artifacts, similar to projection artifacts, were first discussed by Lindmo *et al.* in 1998 [17], where a Monte Carlo simulation program was used to simulate time domain phase-resolved Doppler OCT. Later, a method for reducing the shadowing artifact was reported by Vakoc *et al.* [19] and Mahmud *et al.* [32] where a step-down exponential filtering was proposed to trace the vessels in OCTA during post-processing. In this method, the magnitudes of all the signals below overlying vessel were attenuated according to the magnitude of that overlying flow. As a result, small vessels beneath the overlying vessels would be lost. While the method was designed for 3D vascular data processing, it may not be applicable for *en-face* projection images that are clinically important in ophthalmology. In addition, the method demands computational power, thus is time

#246804 Received 27 Jul 2015; revised 16 Sep 2015; accepted 17 Sep 2015; published 28 Sep 2015

consuming. On the other hand, Makita *et al.* presented a method, similar to Eq. (4), to reduce the shadowing artifacts presented in choroidal vessel visualization using phase-resolved Doppler OCT, i.e., optical coherence angiography, where the steps of normalization, inversion and multiplication were used [18]. The current approach improves this prior treatment by 1) taking the logarithmic compression of OCT signals into the formulation, which is more acceptable in the current commercial OCT systems, and 2) considering the OCT structural information in the minimization of the projection artifacts. The latter could be important because it is believed that retinal structural changes might precede the alternation in blood flow [30]. Thus, the consideration of structural information into the formulation might offer more accurate presentation of CNV involvement in the disease progression. However, it is clear that more clinical CNV cases with necessary statistical power are required to provide a comprehensive evaluation of this proposed method.

One important limitation in the current study is the requirement of appropriate segmentation needed for outer retinal avascular space. Although it is feasible for normal subjects, the automatic segmentation would be difficult for all the patients with CNV, where the clear anatomical layers (boundaries) are not always present. Therefore, we used a semi-automatic segmentation platform in the demonstration of clinical cases, which was time consuming (~3 minutes for one 3D data set). If proved clinically useful, future work is needed to develop automatic segmentation software to accurately segment outer retinal avascular space, so that the method proposed here can be automated for clinical use.

In summary, we have shown that the projection effect due to strong forward- and back-scattering of photons propagating within the blood causes variations in both intensity and phase of OCT signals, leading to tail-like artifacts beneath the functional blood vessels. Even though different angiographic algorithms exist, it is difficult to directly exclude projection artifacts in the OCT based angiography. To solve this problem, we have demonstrated a simple but effective approach to minimize the projection artifacts in angiographic projection images, which may be especially useful for imaging patients with CNV. Due to its easy and straightforward implementation, the proposed method promises a practical use in the clinical OCT based angiography systems. In this study, we have used the fsOMAG algorithm to produce the images of retinal vasculature for the purpose of demonstrating the proposed approach. It should be understood that this approach applies to all the algorithms in the family of OCT based angiography.

Acknowledgment

This study was supported in part by National Eye Institute (R01-EY024158), Carl Zeiss Meditec Inc., and Research to Prevent Blindness (New York, NY). The authors would like to thank Dr. Robert W. Knighton, University of Miami Miller School of Medicine, for his insightful and constructive comments during this study and proof-reading of this manuscript.